Oxide Supported Cobalt Catalysts for CO 2 Hydrogenation to Hydrocarbons: Recent Progress

Canio Scarfiello, Doan Pham Minh, Katerina Soulantica, Philippe Serp

ADVANCED MATERIALS INTERFACES
Open Access
www.advmatinterfaces.de

Oxide Supported Cobalt Catalysts for CO_2 Hydrogenation to Hydrocarbons: Recent Progress

Canio Scarfiello, Doan Pham Minh, Katerina Soulantica, and Philippe Serp**

Carbon capture and utilization represents a promising strategy to meet the global energy and climate goals. Under specific conditions, CO_2 catalytic hydrogenation with renewable H_2 can transform waste CO_2 into a chemical feedstock for added-value energy carriers and chemicals. CO_2-Fischer–Tropsch synthesis-based-hydrocarbons should contribute to the creation of a circular carbon economy with a significant impact on anthropogenic emission into the atmosphere. This review summarizes the progress achieved toward the single-step hydrogenation of CO_2 to long-chain hydrocarbons over oxide-supported Co-based catalysts. Mechanistic aspects are discussed in relation to thermodynamic and kinetic limitations. The main parameters that must be taken into consideration to increase the activity and the selectivity toward compounds of two or more carbon atoms (C_{2+}) are discussed in detail: cobalt active phase, support and metal-support interfaces, and promoters. Finally, particular focus is dedicated to the role of reducible oxide supports and their surface defects on the activation of CO_2, as well as on the regulation and evolution of metal-support interactions.

1. Introduction

The current concentration of CO_2 in the atmosphere is ≈410 parts per million (ppm) and is expected to reach 950 ppm by the end of the century, triggering significant changes in the earth's atmosphere.[1] Over 40% of world's total CO_2 emissions come from fossil fuels, which combustion accounts for 80–90% of world's power generation.[1] From a rational point of view, "prevent" is better than "cure" and consequently, a transition toward carbon-free renewable sources is on the way.[2] This will require decades, huge investments, and significant political as well as technological efforts. Furthermore, some sectors such as carbon-intensive industries (i.e. cements and chemicals industries), intrinsically produce CO_2.[3] In this context, carbon capture and utilization (CCU) represents a promising strategy to meet the global energy and climate goals. Under specific conditions, CO_2 hydrogenation with renewable H_2 can transform waste CO_2 into a chemical feedstock for added-value energy carriers and chemicals.[2,3] In this optic, catalytic hydrogenation of CO_2 received increasing scientific attention over the last decades. Most researchers focused their attention on the hydrogenation to C_1 products such as methane and methanol, which can nowadays be obtained by established industrial by established industrial-scale technologies.[2,4] Conversely, the production of C_{2+} hydrocarbons is more challenging due to the high C—C coupling barrier, and the numerous competing reactions generating C_1 products.[4] However, compounds of two or more carbon atoms (C_{2+}) possess higher volumetric energy densities, which increase with the chain length, and can be easily transported off-grid.[2–4] Reductive C=O bond cleavage of the CO_2 molecule requires a high energy input of ≈750 kJ mol^{-1}. Should this energy effort be paid, the production of higher-value products in a single stage is more interesting than the partial or total hydrogenation into C_1 products.[2] C_{2+} hydrocarbons can be currently produced via the Fischer–Tropsch synthesis (FTS) process using syngas (gas mixture rich in CO and H_2) as feedstock. Compared to petroleum-based products, ultra-clean FTS-based hydrocarbons are free of sulfur, nitrogen, aromatics, and other poisoning species, and can be directly used in subsequent refining processes or immediate commercial applications.[5] CO_2-FTS-based hydrocarbons would allow the creation of a circular carbon economy with a significant impact on anthropogenic emission into the atmosphere. Provided that

C. Scarfiello, D. Pham Minh
Université de Toulouse
IMT Mines Albi
UMR CNRS 5302
Centre RAPSODEE
Campus Jarlard, Albi, Cedex 09 81013, France
E-mail: canio.scarfiello@mines-albi.fr
C. Scarfiello, K. Soulantica
LPCNO
Université de Toulouse
CNRS
INSA
UPS
135 avenue de Rangueil, Toulouse 31077, France
C. Scarfiello, P. Serp
LCC
CNRS-UPR 8241
ENSIACET
Université de Toulouse
4, allée Emile Monso – CS 44362, Toulouse, Cedex 4 31030, France
E-mail: philippe.serp@ensiacet.fr
The ORCID identification number(s) for the author(s) of this article can be found under https://doi.org/10.1002/admi.202202516.

DOI: 10.1002/admi.202202516

CO_2-FTS is conducted under the same industrial conditions, with the same catalysts and product distribution as traditional FTS, the process would be extremely competitive. Due to their high C—C coupling activity in the FTS process, cobalt-based catalysts are good candidates for direct CO_2 hydrogenation to C_{2+} hydrocarbons. Nevertheless, unmodified Co-based catalysts act differently when CO_2 substitutes CO in the feed, producing mainly methane. However, it is known from the 50's that alkalized cobalt catalysts can be active for the catalytic hydrogenation of carbon dioxide to higher hydrocarbons.[6] Since then, it was proposed that a careful choice of the metal oxide support, of the alkaline metal promoters, and regulation of the metal-support interface can enhance the intrinsically marginal activity of Co-based catalysts for the reverse water-gas shift reaction (RWGS), and decrease excess methanation. Similarly, despite their higher activity for RWGS, Fe and Fe-Co based catalysts require careful design and promoter addition to improve their activity and selectivity toward C_{2+} products.[7–10] Moreover, due to their lower hydrogenation ability, such catalysts produce more olefins and oxygenates products.[7–10]

Here we present an overview of the progress achieved toward the single-step hydrogenation of CO_2 to long-chain hydrocarbons over oxide-supported Co-based catalysts. Mechanistic aspects are discussed in relation to thermodynamic and kinetic limitations. The main parameters that affect the activity and the selectivity toward C_{2+} products are discussed in detail: cobalt active phase, support and metal-support interfaces, and promoters. Finally, particular focus is dedicated to the role of reducible oxides as supports and their surface defects on the activation of CO_2, as well as on the regulation and evolution of metal-support interactions.

2. Thermodynamic and Kinetic Restrictions Over Metallic Cobalt Catalysts

Metallic cobalt, especially in its hexagonal close-packed (hcp) phase, represents one of the best choices for the conversion of syngas to hydrocarbons via FTS.[5] Due to their superior chain-growth capability, high stability and low activity for the water-gas shift (WGS) reaction, Co-based catalysts are typically employed in the low temperature FTS process (220–250 °C) to produce heavy hydrocarbons with a high carbon efficiency.[4,5] This surface polymerization reaction leads to a hydrocarbon product pattern that can be ideally modeled by an Anderson–Schulz–Flory (ASF) distribution (**Figure 1**), mathematically expressed as $W_n = n(1-\alpha)^2\alpha^{n-1}$,[2] where W_n represents the weight fraction of products with n carbon atoms in their chain, and α is the chain-growth probability. According to the ASF distribution, only CH_4 and C_{21+} hydrocarbons can be obtained with high selectivity at low and high α value, respectively.[5] Conversely, a careful control of α is necessary to directly obtain specific middle-distillate hydrocarbons.[5] Due to such restrictions, Co-based catalysts are traditionally employed in FTS to maximize the production of heavy hydrocarbons (C_{21+}, $\alpha > 0.9$), which, in turn, are converted into the desired middle distillate mix blend via a downstream hydrocracking refining treatment.[5]

The utilization of such a process for the direct synthesis of CO_2-based heavy hydrocarbons would represent an important

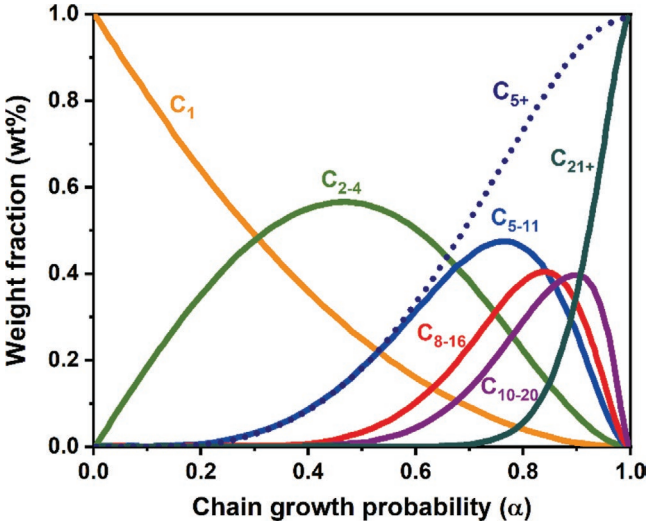

Figure 1. Weight fractions of different hydrocarbons as a function of the chain-growth probability (α) assuming an ideal ASF distribution. Source: C. Scarfiello.

route toward greener high-density chemical energy storage. Cobalt seems to be the obvious choice for such a purpose, and therefore, over the years several attempts were made by simply switching the feed composition from CO to CO_2 with traditional Co-based FTS catalysts.[11–13] Unfortunately, under industrial relevant operation conditions, the progressive substitution of CO by CO_2 in the feed results in limited CO_2 conversion levels (<20%) and increased methane selectivity (>70%). Moreover, the chain-growth probability for C_{2+} hydrocarbon precursors significantly decreases, leading to the production of shorter chain products ($\alpha < 0.5$–0.6).[2,11–14] Such undesired outcomes can be ascribed to thermodynamic limitations that have direct kinetic consequences.[2,14] Indeed, during CO_2 hydrogenation to hydrocarbons, the FTS reaction (R2) occurs only in a second time, after the initial transformation of CO_2 into CO via the RWGS (R1):

$$\begin{aligned}
&(R1)\ CO_2 + H_2 \rightarrow CO + H_2O && \Delta H_{298} = 41.2\,kJ\cdot mol^{-1} && \text{RWGS}\\
&(R2)\ nCO + (2n+1)H_2 \rightarrow C_nH_{2n+2} + nH_2O && \Delta H_{298} = -165\,kJ\cdot mol^{-1} && \text{FTS}\\
&(R3)\ CO_2 + 4H_2 \rightarrow CH_4 + 2H_2O && \Delta H_{298} = -164.8\,kJ\cdot mol^{-1} && \text{Sabatier}\\
&(R4)\ CO + 3H_2 \rightarrow CH_4 + H_2O && \Delta H_{298} = -206\,kJ\cdot mol^{-1}
\end{aligned} \quad (1)$$

As the RWGS is a slightly endothermic reaction, CO_2 conversion to CO is limited at the low temperatures required for the traditional FTS. Indeed, for a H_2/CO_2 ratio of 3 (stoichiometric ratio for CO_2 hydrogenation to $-CH_2-$), and temperatures between 220 and 300 °C, only 13–23% of CO_2 can be converted to CO.[14] As the exothermic FTS has no thermodynamic constraint in this temperature range, the consecutive reaction of the CO can lead to higher CO_2 conversion for the overall process, provided that the reaction rate of FTS is equal to or higher than that of the RWGS.[14] Moreover, the competitive exothermic formation of methane from CO_2 (R3) and CO (R4) is highly favored.[14] Therefore, as traditional Co-based FTS catalysts are not particularly active for the RWGS, they mainly act as methanation catalysts under CO_2/H_2 feeds, and important modifications are needed to modulate such a behavior.[2,14] Careful choice

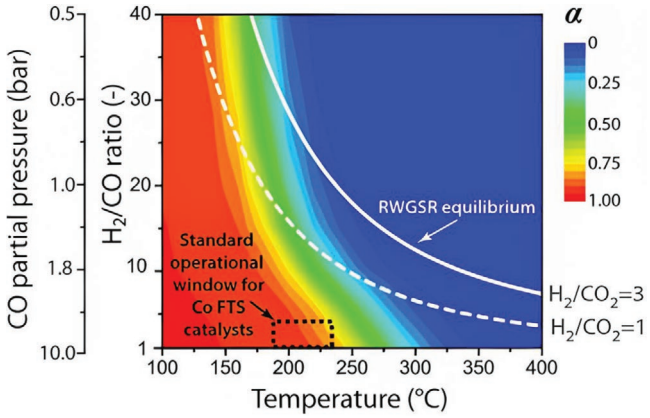

Figure 2. Contour plot for the hydrocarbon chain-growth probability (α) on a cobalt-based FTS catalyst, as a function of the reaction temperature and H_2/CO ratio (or CO partial pressure) at a constant total pressure of 20 bar. The white lines represent the equilibrium compositions for the RWGS reaction starting from feeds with different H_2/CO_2 molar ratios. The standard operational window for cobalt-based catalysts employed in syngas ($CO+H_2$) FTS is indicated by the dashed frame. Reproduced with permission.[2] Copyright 2017 Wiley-VCH Verlag GmbH & Co. KGaA, Weinheim.

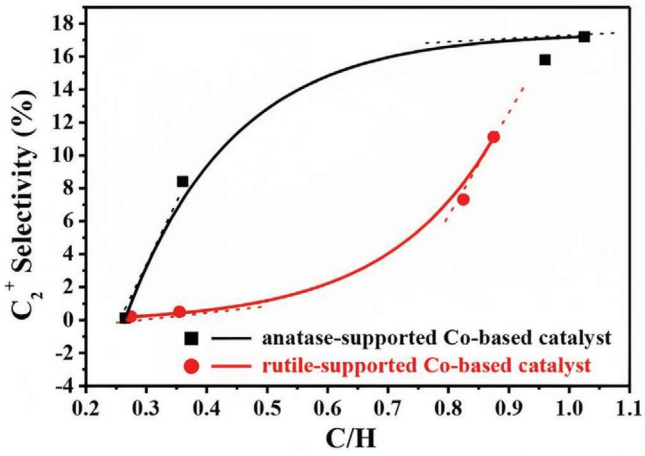

Figure 3. C_{2+} selectivity as a function of C/H ratio over anatase and rutile Co/TiO_2 catalysts. Reproduced with permission.[20] Copyright 2019, American Chemical Society.

of the metal oxide support, alkaline metal promoters and regulation of the metal-support interface can enhance the intrinsically marginal activity of Co-based catalysts for the RWGS, and decrease excess methanation. The thermodynamic constraint of the RWGS also sets important limitations to the chain propagations on cobalt catalysts, leading to the experimentally observed production of shorter chain hydrocarbons. As discussed by Prieto,[2] and summarized in the **Figure 2**, in the most favorable case for RWGS, under H_2/CO_2 feed ratio between 1 and 3 and a total pressure of 20 bar, only H_2/CO molar ratios above 10 and, therefore, CO partial pressure (P_{CO}) lower than 1.8 bar are possible. Such a low CO partial pressure set by the RWGS equilibrium limits the chain-growth probability to values below 0.5–0.6, that is far from the industrially relevant α values (>0.8) achievable at relatively high P_{CO} (>10 bar) under traditional FTS conditions.[2] The reasons behind the considerable dependence of the chain-growth probability on P_{CO} are not completely clear, but they seem to be related to small variations of the CO coverage (θ_{CO}) on the metallic cobalt surface. Indeed, under subatmospheric CO partial pressure, Co-based FTS catalysts mainly produce methane, despite the fact that θ_{CO}, independent of P_{H2}, is close to saturation. Conversely, high chain-growth probabilities are obtained upon marginal increase of θ_{CO} at industrially relevant conditions (>5 bar).[2,15,16] According to density functional theory (DFT) calculations, for a CO insertion chain-growth mechanism (Pichler–Schultz mechanism), a very high θ_{CO} on FTS cobalt catalysts plays a pivotal role in the destabilization of $*CH_x$ (x = 1–2) species, thus facilitating the insertion of CO into these surface species, a key step for chain growth.[2,17] Similarly, DFT simulations on Ru-based FTS catalysts reveal that H-assisted *CO dissociation in proximity of growing $*C_xH_y$ chains is an essential step for chain propagation.[2,18] Therefore, quasi-saturation CO coverages can lead to preferential dissociation of CO (monomer) in the proximity of a few growing chains, leading to high effective chain-growth probability.[2,18]

Bredy et al. recently confirmed the relationship between θ_{CO} on metallic Co (supported on TiO_2 and Siralox) and selectivity toward higher hydrocarbons via *operando* diffuse reflectance spectroscopy (DRIFTs).[19] The selectivity to methane increases monotonously with decreasing θ_{CO} when CO_2 is introduced in the feed alongside CO. Moreover, the structure and oxidation state of the surface of metallic cobalt remains the same whether CO_2 or CO are co-fed with H_2, thus confirming that a high θ_{CO} is the key feature to achieve high selectivity for hydrocarbons during CO_2 hydrogenation. According to Visconti et al.,[13] the different selectivity between CO and CO_2 feeds are related to the different adsorption strengths of the two molecules, which lead to different C/H ratios on the catalyst surface. The weaker CO_2 adsorption on metallic cobalt results in a higher local hydrogen fractional coverage, which favors chain termination. Li et al. have proved that the increase of C/H ratio by the addition of promoters (K, Zr, Cs) results in higher C_{2+} selectivity over Co/TiO_2 catalysts (**Figure 3**).[20]

Hence, thermodynamic restrictions strongly limit the applicability of traditional Co-based catalysts for the direct production of long chain hydrocarbons under CO_2/H_2 feed. Significant structural modifications are thus needed to furnish the Co catalysts with active species that can promote the RWGS under industrially relevant conditions, to increase their activity and limit methane production.

Nevertheless, even in combination with effective RWGS functionalities, CO fugacity strongly affects chain-growth probability, leading to the production of shorter chain hydrocarbons (α < 0.5–0.6). Therefore, Co-based catalysts might be used for the direct production of synthetic natural gas mixtures rich in light C_2-C_4 hydrocarbons, and CO_2-based middle distillate mix (i.e., gasoline, jet fuel, and diesel) without the necessity of a downstream hydrocracking refining treatment.

3. Cobalt Active Phase

Metallic cobalt can exist in three different crystal phases: α-Co (hexagonal-close-packed, hcp), β-Co (face-centered-cubic, fcc),

and ε-Co (cubic-primitive, cp).[21–25] The latter is a metastable phase and can easily be transformed into hcp-Co and fcc-Co, which are the most common crystal phases for traditional FTS catalysts.[21–26] A phase transition from the low temperature hcp-Co phase to the high temperature fcc-Co occurs at ≈400 °C in bulk cobalt,[21,27] but can take place at lower temperatures (≤300 °C) for metal nanoparticles (NPs).[28] hcp-cobalt NPs present higher FTS activity due to the more favorable direct dissociation of CO, while H-assisted CO dissociation takes place on fcc-cobalt.[21] However, hcp-Co seems to be less resistant to water-induced re-oxidation and cobalt carbide formation.[21] It is generally admitted that for the traditional FTS, the optimum metallic cobalt NP size is between 6 and 10 nm, depending on the catalyst type and reaction conditions.[5] Below this range, Co NPs generally produce more methane and are more prone to re-oxidation.[21] Above this value, turnover frequency (TOF) is generally lower, and C_{5+} selectivity remains almost unchanged.[5,21,29]

Regarding CO_2-FTS, most of the metallic Co-based catalysts contain fcc-cobalt. To the best of our knowledge, a robust comparison between hcp- and fcc-cobalt NPs supported on a metallic oxide doesn't exist in the current literature. However, such a study has been carried out for unsupported hcp- and fcc-cobalt NPs by Li et al.[30] Under a molar ratio of $H_2/CO_2 = 4$ and a pressure of 30 bar, hcp-Co shows higher activity than fcc-Co. CO_2 dissociates directly into chemisorbed CO* and O* on both cobalt phases, but the different adsorption strengths of the CO* intermediate lead to different product selectivity. On hcp-Co, strongly adsorbed CO* is hydrogenated to methane, while over fcc-Co, due to a weaker adsorption, it easily desorbs to produce gaseous CO.

The effect of cobalt particle size on CO_2 hydrogenation is still significantly understudied and will likely become an important discussion topic in the future. It has been reported that for CO_2 hydrogenation, 10 nm Co particles supported on mesoporous silica (MCF-17) display higher TOF than 3 and 7 nm ones.[31] On the other hand, no significant differences in terms of product distribution are detected at a pressure of 6 bar and H_2/CO_2 ratio of 3.[31] Similarly, for a promoted Co-Na-Mo based catalyst, NPs smaller than 2 nm supported on MgO show low RWGS conversion and negligible FTS activity.[32] Larger Co NPs (≈15 nm) supported on SiO_2 and ZSM-5 lead to higher CO_2 conversion and hydrocarbon selectivity.[32] Finally, further increase of Co NPs size to 25–30 nm has a detrimental effect on the global CO_2 conversion.[32]

Metallic cobalt is generally accepted as the active phase during traditional FTS, and is the most studied cobalt phase for CO_2-FTS as well.[5,21] However, metallic cobalt and cobalt oxides often coexist under FTS conditions;[21] and, in 2014, evidences of a highly active cobalt oxide catalyst (CoO/TiO_2) for the FTS and CO_2-FTS reactions were presented by Melaet et al.[33] The higher activity and selectivity of such catalyst were ascribed to the formation of an active and unique interface between CoO and the TiO_2 support. Similar results were obtained in a more recent and complete study on the activity and selectivity of metallic Co and CoO supported on reducible (CeO_2 and TiO_2) and non-reducible (SiO_2 and Al_2O_3) metal oxides.[3] Metallic cobalt is more active than CoO, except when supported on TiO_2 P25 (a mixture of rutile and anatase TiO_2 phases). CoO/TiO_2 produces also more C_{2+} products compared to its metallic counterpart, with a higher content of olefins, due to its lower hydrogenation ability. Conversely, Co/TiO_2 exclusively produces paraffins. DRIFTs analysis highlights that metallic Co catalysts follow the direct dissociation mechanism, indicated by the presence of adsorbed CO as intermediate. The latter is not present on CoO catalysts, which instead favor a H-assisted mechanism (**Figure 4**), characterized by formyl, formate and carbonate intermediates.[3] These results are in good agreement with theoretical works, which found that CO adsorption is strong on metallic Co (−1.99 eV = −192 kJ mol^{-1}) and weak on CoO (−0.33 eV = −32 kJ mol^{-1}).[3,34] Kinetic insights reveal that direct dissociation occurs at higher rate than H-assisted pathway. Thus, CoO-based catalysts can benefit from a higher H_2 partial pressure, which is instead detrimental for metallic cobalt ones.

Wang et al.[35] have recently shown that, for cobalt active species, the regulation of their valence state can lead to a different selectivity during CO_2 hydrogenation. According to this study, CoO particles are extremely active for the production of CO via RWGS, while metallic Co species promote methanation.[35] FTIR characterization highlights that, on CoO, adsorbed formates are key intermediates for the formation of CO. Conversely, on Co^0 sites, the carboxylate intermediate evolves to

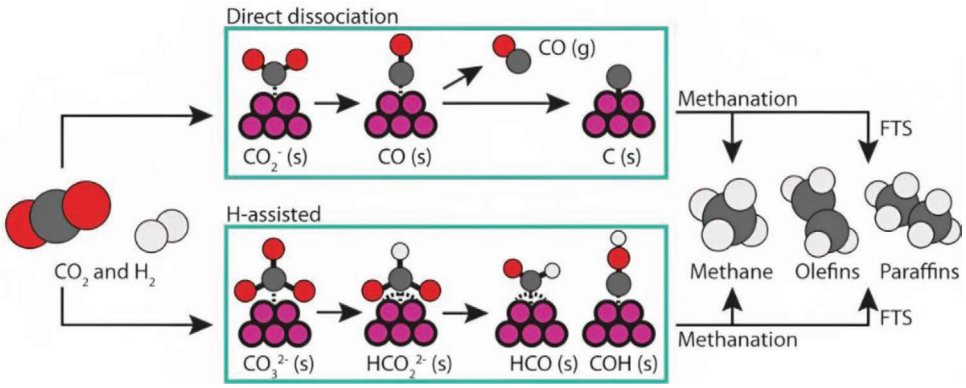

Figure 4. Simplified reaction pathways for CO_2 hydrogenation to hydrocarbons over Co-based catalysts. In the direct dissociation mechanism, the CO_{ads} intermediate can either desorb or form C_{ads} and then hydrocarbon products. The H-assisted pathway involves surface carbonates, formates, and formyl as intermediates. The latter can either be fully hydrogenated to methane or converted into olefins or paraffins via C—C coupling (FTS). Reproduced under terms of the CC-BY license.[3] Copyright 2022, The Author(s), published by Springer Nature.

adsorbed CO, which in turn is hydrogenated to CH_4.[35] Notably, weak CO adsorption on CoO favors its desorption. Stronger CO adsorption on metallic Co, along with higher surface hydrogenation resulting from enhanced H_2 activation, leads to CH_4 formation.[35]

Indeed, metallic Co is more active than CoO for H_2 dissociation, leading to a high amount of surface-active H species.[36–38] Moreover, the high electron density near the Fermi level provides Co^0 with excited electrons for the different hydrogenation steps.[36,39] Both DFT and experimental results show better CO_2 activation on Co than on CoO.[3,36,39] Additionally, $Co^{\delta+}$ sites at CoO_x–CeO_2 interface limit formate hydrogenation to methane,[40] while the synergy between Co and Zr in uniform Co-O-Zr sites accelerates the decomposition of formates to CO, leading to superior RWGS performances.[35,41] CoO can be obtained via a controlled reduction,[3] or can be formed in situ via re-oxidation of small metallic cobalt NPs.[21] Finally, CoO can be stabilized via strong metal support interaction (SMSI), as illustrated in the following section of this review.[3,21,33] As CoO seems to be particularly active for RWGS reaction, while metallic Co is known for is optimal CO-FTS selectivity, a close cooperation between these different active sites might lead to superior CO_2-FTS selectivity toward long chain hydrocarbons. However, as summarized by Lin et al.,[5] "synergistic dual site" in close proximity, namely Co^0-Co_2C,[42–44] Co^0-$Co^{\delta+}$,[45,46] or Co-Co^{2+}/Co_2C,[47] can promote the formation of higher alcohols. The metallic cobalt is necessary for the initial CO cleavage and the consecutive formation $*CH_x$ species.[5] The second site, most likely a carbide, although it has been proposed to work also with $Co^{\delta+}$/Co^{2+}, is necessary for the non-dissociative adsorption and insertion of CO.[5] However, the fabrication of stable dual site structures remains a challenge.[5]

Besides metallic and oxide cobalt, cobalt carbide can also be formed during traditional CO-FTS.[21] The role of this phase is quite controversial, as some studies correlate its presence to the formation of olefins and oxygenates,[21,43,48–50] while others to catalyst deactivation.[21,51–53] As previously mentioned, cobalt carbide is an active site for CO non-dissociative adsorption and insertion in dual site structures during the formation of higher alcohols.[5,36] According to Yu et al.,[54] a Co_2C/γ-Al_2O_3 catalyst is very active for CO_2 methanation, with a CH_4 selectivity close to 100%. Additionally, Khangale et al.[55] suggest that the formation of Co_2C in a Co-K/Al_2O_3 catalyst is responsible for catalyst deactivation and increasing CH_4 formation with increasing reaction time. However, recent works report that a simple morphological modulation of Co_2C nanoprisms can lead to excellent low-temperature RWGS or cascade RWGS-FTS reaction activity, leading to the production of olefins and alcohols.[56,57] The role of cobalt carbides in CO_2 hydrogenation is still significantly understudied and will likely become an important discussion topic in the future.

To summarize, it seems that depending on the support, both metallic cobalt and and cobalt oxide can be active phases during the CO_2-FTS reaction to long chain hydrocarbons. Metallic cobalt is more active on most supports, while CoO is a better choice for TiO_2 support. Such a behavior stems from the formation of a unique interface between the cobalt oxide and the reducible oxide, which will be discussed in more details in the following sections of this review. Moreover, CoO shows interesting activity toward the RWGS reaction. Nonetheless, further investigations are definitively needed to clarify the role of CoO and Co^0-CoO interfaces during CO_2-FTS, as well as the possible formation of cobalt carbide and its consequences on CO_2 hydrogenation.

4. Effect of Support and Metal-Support Interfaces

Due to its utilization in industry, Al_2O_3 is the most extensively studied support for traditional Co-based FTS catalysts.[58] SiO_2, TiO_2, and ZrO_2 have been also largely employed in the preparation of Co-based FTS catalysts.[58] Metal-support interactions (MSI) play a pivotal role on the dispersion, reduction, and activation behavior of the active metal phase.[5] SMSI can lead, mainly through electronic and geometric effects, to different situations. On one hand, we can have the formation of undesired refractory compounds (e.g., CoAl and CoSi) or the complete encapsulation of the active metallic phase.[5,58] On the other hand, it has been shown that charge transfer, metal surface coverage by a thin layer of reducible oxide, and formation of special metal-oxide interfaces can result in highly efficient FTS catalysts.[5,59–62] The latter are common features of reducible metal oxides, which are further characterized by the formation of oxygen vacancies (O_{vac}) on their surface. Oxygen vacancies can be extremely useful for FTS, as they can promote CO_2[63] as well as CO dissociation.[59]

The effect of support and metal-support interfaces is even more important during CO_2 hydrogenation. Recently, ten Have et al.[3] have studied the CO_2 hydrogenation over metallic Co and CoO (≈10 wt%), supported on reducible (CeO_2 and TiO_2) and non-reducible (SiO_2 and Al_2O_3) oxides under CO_2-FTS relevant conditions (T = 250 °C, P = 20 bar, H_2/CO_2 = 3). Cobalt particles size above 10 nm on all the supports (14–17 nm for SiO_2, Al_2O_3 and TiO_2; and 37 nm for CeO_2) avoided interfering size effects on the activity.[3] As already mentioned in the previous section, CoO/TiO_2 is the most active and selective system. However, among the investigated supports, TiO_2 leads to the higher activity even with metallic cobalt NPs (**Figure 5**). The reason lies in the optimum reducibility of the TiO_2 support, which allows the weakening of the CO bond. Indeed, for the reduced Co/TiO_2, a red shift of the CO_{ads} peak (1994, 1992, 1987, and 1980 cm^{-1} for Co/SiO_2, Co/Al_2O_3, Co/CeO_2, and Co/TiO_2, respectively), indicates a weaker CO bond on reducible oxides, as observed by DRIFTS.[3] Moreover, evident and broad signals of surface (bi)carbonates and formates were detected for the catalysts prepared on reducible supports, and not on non-reducible oxides.[3] This is due to the different basicity of the supports (TiO_2 > CeO_2 > Al_2O_3 > SiO_2).[3] CO_2 can interact directly with O^{2-} surface ions and -OH surface groups, leading to the formation of carbonate and bicarbonate species, respectively.[3,64] Formates originate from the interaction of CO_2 with surface O_{vac}, which are easily formed on reducible oxides such as TiO_2 and CeO_2.[3,65] Besides, hydrogen spillover is known to occur ten orders of magnitude faster on TiO_2 than on Al_2O_3.[66] Finally, a peak splitting was observed for carbonates on Co/TiO_2. The latter can be ascribed to different types of coordination and/or different adsorption centers, suggesting the formation of a new interface between Co and TiO_2 with different adsorption features.[3,67–69]

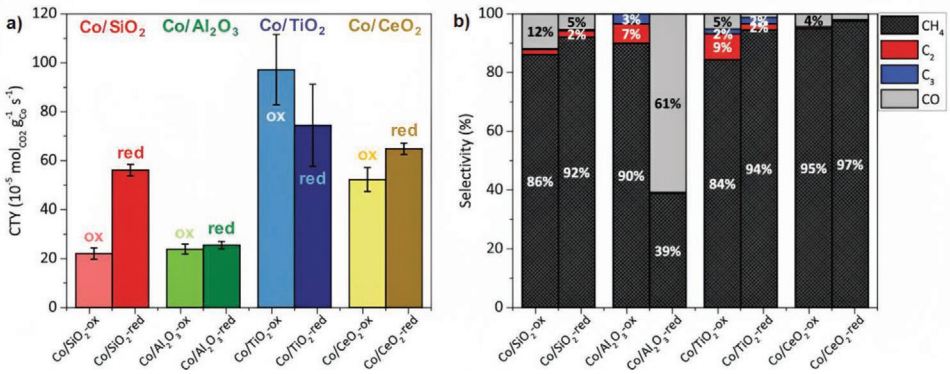

Figure 5. Catalytic activity (cobalt-time-yield (CTY)) (a) and selectivity (b) of Co-based catalysts as CoO (suffix: -ox) and metallic Co (suffix: -red) supported on reducible (CeO_2 and TiO_2) and non-reducible (SiO_2 and Al_2O_3) oxides. Reaction conditions: T = 250 °C, P = 20 bar, H_2/CO_2 = 3. Time-on-stream = 10 h. Reproduced under terms of the CC-BY license.[3] Copyright 2022, The Author(s), published by Springer Nature.

In addition, metal oxide supports with the same chemical composition but different crystal phases can strongly affect the catalytic performance of the final catalysts,[20,70] both in terms of activity and selectivity. The support allowing the higher activity and selectivity of the previous study[3] is a commercial TiO_2-P25, which contains a mixture of anatase (80%) and rutile (20%). Cobalt catalysts with the same metal loading (≈10 wt%) and particle size (20 nm) were investigated on the two pure TiO_2 crystal forms by Li et al.[20] Co/rutile-TiO_2 catalyst shows higher activity and selectively for CO_2 hydrogenation to CH_4. Conversely, Co/anatase-TiO_2 catalyst has a lower CO_2 conversion, and produces mainly CO. By simply increasing the calcination temperature of the anatase-TiO_2 at 800 °C, the product selectivity completely changes from CO to CH_4, and the CO_2 conversion increases to the same values of the catalyst prepared on the rutile-TiO_2 support. Such a change is due to the surface phase transition of anatase to the rutile phase, thus confirming the pivotal role of the support crystal phase.[20] DRIFTs and temperature programed desorption (TPD) characterizations suggest that the different activity and selectivity can mainly be attributed to the different ability of anatase and rutile to adsorb CO_2, CO, and H_2. Indeed, the weak bond of *CO intermediate over Co/anatase-TiO_2 leads to its immediate desorption as gas-phase CO, and negligible CO_2 conversion. Conversely, stronger adsorption on Co/rutile-TiO_2 enables the formation of the key intermediate formate species, which are further converted to CH_4, along with higher CO_2 conversion.[20] The modification of such catalysts by addition of different promoters (K, Zr, and Cs) leads to stronger adsorptions, allowing increasing surface C/H ratio, and consequently the C_{2+} selectivity (Figure 3). For the rutile-based catalysts, the C_{2+} selectivity increases slowly at low C/H ratio < 0.5, and quickly at C/H > 0.5. Distinctly, on anatase-based catalysts, higher increase occurs at C/H < 0.5 and lower at C/H > 0.5.[20] Notably, anatase-supported catalysts always have higher C_{2+} selectivity than the rutile-based ones, even at the same C/H ratio. The higher C_{2+} selectivity of anatase supported catalysts is attributed to specific metal-support interactions. Additionally, for both catalysts Co NPs are covered by a thin TiO_2 overlayer, the thickness of which can vary from 2 to 4 nm depending on the calcination treatment. X-Ray photoelectron spectroscopy (XPS) also reveals the presence of anion vacancies and defects that can adsorb and activate CO_2 and CO.[20]

As mentioned in the previous section, in 2014, Melaet et al.[33] reported a particularly active CoO/TiO_2 catalyst. In their work, 10 nm Co NPs are prepared via colloidal route and then dispersed on macroporous TiO_2 and mesoporous SiO_2 (MCF-17). Over the SiO_2 support, metallic cobalt shows higher TOF than CoO during both CO_2 (H_2/CO_2 = 3) and CO (H_2/CO = 1) hydrogenation at 250 °C and 5 atm of pressure. Conversely, for the TiO_2 support, CoO performs better than its metallic counterpart, despite a higher olefin production due to the lower hydrogenation ability.[33] To obtain CoO and metallic Co, the samples are treated under H_2 at 250 and 450 °C, respectively. XPS characterizations demonstrate that after the treatment at 250 °C in H_2, the content of Co on the surface is equal to 29 atomic %, and drops to 20 atomic % at 450 °C. Additionally, at 250 °C, Ti on the surface is only partially reduced, whereas full reduction to Ti^{3+} is achieved at 450 °C. Therefore, the high temperature reduction leads to an encapsulation of the metallic Co active phase, while CoO wetting of the support takes place at 250 °C (**Figure 6**).

The latter enables the formation of an extended unique interface between CoO and TiO_2 with enhanced activity for CO and CO_2 hydrogenation.[33]

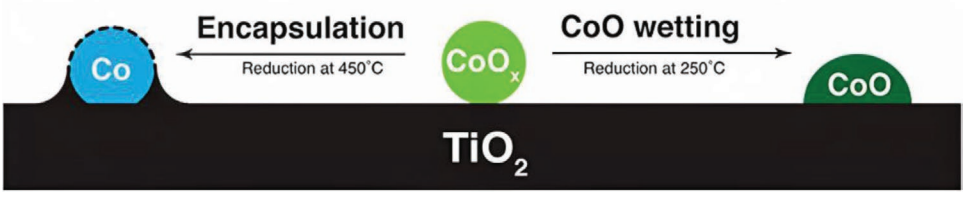

Figure 6. Metallic Co encapsulation and CoO wetting over TiO_2 after reduction at 450 and 250 °C, respectively. Reproduced with permission.[33] Copyright 2014, American Chemical Society.

As illustrated by Khangale et al.,[71] an unpromoted 15 wt% Co/ZrO_2 catalyst produces mainly methane with a selectivity of 99.4%, which decreases upon K promotion. For promoted Co-Na-Mo catalysts, the systems involving CeO_2 and TiO_2 supports provide higher α values than the ones prepared on SiO_2, Al_2O_3, MgO, ZrO_2, and ZSM-5.[32]

Therefore, the effect of the support is extremely important during CO_2 hydrogenation to hydrocarbons. Independently from the cobalt active phase, catalysts prepared on reducible oxides, and especially TiO_2 are more active than those prepared on irreducible oxides.

On one hand, the higher activity stems from the ability of reducible oxides to create specific metal-support interfaces, originating from SMSI, which can strongly benefit CO_2 activation to different products, from C_{2+} to CH_4 and CO. For instance, Co/CeO_2 catalysts show superior performance for CO_2 hydrogenation to CH_4 due the formation of O_{vac},[72] and higher reducibility linked to Co-CeO_2 interactions.[73] Additionally, the selectivity of Ir/TiO_2 catalysts can be completely changed from CH_4 to CO thanks to the formation of a reduced TiO_x overlayer around Ir NPs.[74] To benefit from SMSI, it is necessary to find the optimum interaction strength that allows the formation of highly active interfaces, without inducing complete encapsulation that can be extremely detrimental.[75] A more detailed analysis of SMSI and its evolution for the most active system (Co/TiO_2) is given in the section 4.3.

On the other hand, reducible oxides are rich of surface defects that can be exploited for the direct activation of CO_2, CO, and H_2. Moreover, defects can play important roles during the preparation of Co-based catalysts, from direct reduction of the different cobalt precursor to the promotion of SMSI. A more detail analysis of these effects is available in the sections 4.1 and 4.2.

4.1. CO_2 Activation Over Surface Defects

CO_2 is a linear non-polar molecule with two equivalent C=O double bonds and a high oxidation state of carbon (+4) that makes it thermodynamically very stable. Therefore, reductive C=O bond cleavage requires a high energy input (≈750 $kJ{\cdot}mol^{-1}$), which can be reduced via a proper activation.[76] CO_2 activation generally involves altering the molecular properties, such as the C=O bond length or O=C=O angle, and can occur both nucleophilically and/or electrophilically through the carbon or oxygen atom, respectively.[76] Generally, the activation of CO_2 molecule over heterogeneous catalysts involves its adsorption, followed by an electron transfer from the catalyst to the molecule. In such a route, metal NPs can serve as active sites for full or partial transfer, leading to the formation of CO_2^- or $CO_2^{\delta-}$, respectively. The interaction of CO_2 with single metals is generally weak, but can be improved by the addition of promoters (e.g., alkali[76–78]), or the formation of alloys.[76] However, some metals (Fe, Ni, and Co) can activate CO_2 more strongly as single metals than as constituents of an alloy.[76,79] On cobalt, DFT calculations demonstrated that CO_2 activation depends on particle size: Co_{55} nanoclusters show higher CO_2 dissociation activity than Co_{13} and Co_{38}.[80] Additionally, CO_2 dissociation becomes easier for all metallic clusters in the presence of H_2.[81]

On the surface of stoichiometric metal oxides, CO_2 activation can occur over both metal (M^{n+}) and oxygen (O^{2-}) ions. It can take place via coordination of CO_2 terminal oxygen atoms to one or two adjacent metal ions, while the carbon atom of CO_2 can interact with surface oxygen sites. These interactions result in monodentate or bidentate carbonate species. CO_2 activation can also occur via the σ-bond or π-bond activation on metal and oxygen ions, respectively.[76,82] On defect-rich non-stoichiometric metal oxides (e.g., TiO_{2-x}, CeO_{2-x}, etc.), O_{vac} can interact directly with carbon and oxygen atoms of CO_2, leading to enhanced CO_2 adsorption. According to DFT calculations, CO_2 adsorption on reduced ceria (110) is thermodynamically favored compared to adsorption on the stoichiometric ceria (110) surface.[76,83] Similarly, CO_2 is preferentially adsorbed at the O_{vac} defects of the TiO_2 (110) surface.[76,84] On the stoichiometric TiO_2 (001) surface, CO_2 dissociation is not observed, and only monodentate carbonate species can be obtained via DFT.[63,76] The introduction of O_{vac} defects generates new adsorption configuration with the formation of a CO molecule, which can easily desorb.[63,76] CO_2 chemisorption was also studied at room temperature using in situ DRIFTs. Besides the carbonate and bicarbonate species resulting from the interaction with the oxygen sites, CO_2 chemisorption is also observed at Ce^{3+}, Ce^{4+}, Ti^{3+}, and Ti^{4+} sites.[76,85] Therefore, O_{vac} can enhance CO_2 adsorption and dissociation via the creation of a high number of stronger binding sites.[86] Additionally, O_{vac} can promote specific reaction pathways, via stabilization of key intermediates. Bobadilla et al.[87] investigated the RWGS reaction on Au/Al_2O_3 and Au/TiO_2 catalysts. On both catalysts, CO_2 initial activation occurs on the supports, as Au NPs are not able to promote direct dissociation to CO and O.[87] In the case of Au/Al_2O_3, CO_2 initially adsorbs on the hydroxyls of the Al_2O_3 to generate bicarbonate species. Then, H atoms activated on gold spill over to the support to react with the bicarbonates, leading to the formation of "fast formates," which can finally decompose to CO.[87] Conversely, on the reducible TiO_2 support, the reaction proceeds at lower temperatures via a redox mechanism involving the direct participation of Ti^{3+}, surface hydroxyl and O_{vac} to form hydroxycarbonyl intermediates, which further decompose to CO and water (**Figure 7**).[87]

A direct correlation between the relative concentration of O_{vac} on the TiO_2 support and the RWGS reaction rate was evidenced. Moreover, a low level of CO production was observed during a reference catalytic test using bare TiO_2, highlighting that CO_2 activation can takes place also in absence of Au species.[87] Thus, the main role of the metal NPs is the H_2 activation, and its subsequent spillover to the TiO_2 surface to increase the number of O_{vac} for CO_2 activation.[87] In this respect, the formation of O_{vac} is highly favored at the metal-oxide interface. This is not only due to the increased presence of highly reducing H species,[87] but also to the higher reactivity of the O atoms at the boundary region.[88] The latter can be more easily removed in comparison to the other O atoms of the surface. Indeed, the electron density of the reduced system tends to be localized on undercoordinated cations (e.g., Ce^{3+}), which are largely present at the nanoscale.[88] Moreover, nanostructures are in general more flexible than extended surfaces or bulk materials: atomic relaxation around the O_{vac} occurs at lower costs, thus stabilizing the defect.[88] Finally, the proximal metal

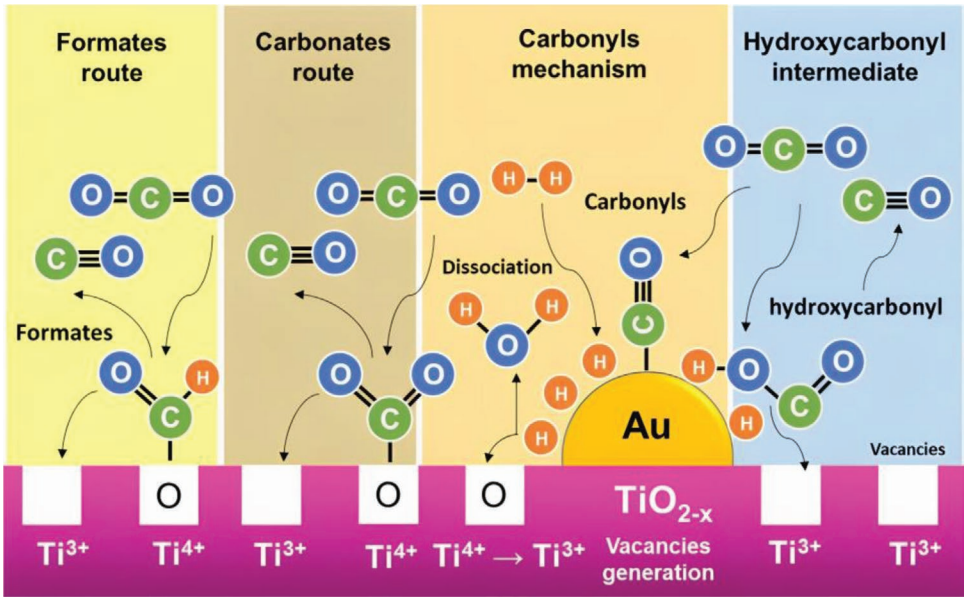

Figure 7. Suggested mechanism for RWGS reaction over Au/TiO_2 catalysts. Reproduced with permission.[87] Copyright 2018, American Chemical Society.

NPs play a pivotal role in delocalizing the excess of electrons, resulting from the generation of a neutral vacancy.[88]

Hence, providing Co-based catalysts supported on reducible oxides with large number of O_{vac} can be a useful strategy to increase the activity for CO_2 hydrogenation, and tune the selectivity toward the desired products. A comprehensive description of the different techniques for creating O_{vac} is beyond the scope of this review. However, the reader can find several examples in the literature concerning O_{vac} formation and characterization over CeO_2[1,89] and TiO_2.[90–93]

4.2. Defect Mediated Reduction/Growth of Metal Nanoparticles

Besides their ability to directly activate CO_2, surface defects on reducible oxides can also play an important role during the preparation of supported catalysts. Indeed, the electrons located on the O_{vac} can directly interact with the ionic metal precursors via an in situ redox reaction, leading to the spontaneous formation of metallic NPs. As such process does not require any foreign reducing agents or stabilizing molecules, and it takes place in a single step, it can be exploited for the preparation of several metal/semiconductor composites, with superior performance during both photo[94–96] and thermal catalysis.[97] Moreover, the metal particle size can be controlled by different parameters, from the amount of metal precursors[94] to the amount of surface defects,[97] as both these parameters can affect the nucleation and growth kinetics of metal NPs. Certainly, the possibility of controlling the metal particle size by tuning the amount of surface defects is the most interesting option. A negative correlation between Pd dispersion and surface defects concentration was highlighted by Cao et al.[97] Indeed, on a low-defect CeO_2 support, the strong electrostatic interaction with the metal precursor (with the consequent formation of many Pd nuclei), and the weak reducing capacity of the support lead to the formation of smaller particles. Conversely, the fewer Pd nuclei and the faster growth on the defect rich CeO_2 lead to the formation of larger Pd NPs. The latter show also higher electron density than smaller NPs. Such electron enrichment, due to SMSI, favors the H_2 activation and consequently the spillover, which in turn contributes to the in situ formation of O_{vac} for CO_2 activation. Further evidence of the SMSI formation during the defect mediated reduction of metal precursor resides in the presence of gold NPs partially embedded in the surface of TiO_2, as demonstrated by Pan et al.[95] The SMSI is known to play a crucial role in regulating the catalytic activity, the selectivity and the stability of metal NPs supported on reducible oxides. It is also known that the existence of O_{vac} on the TiO_2 surface, either from reduction or doping, can largely favor decoration and encapsulation of Pd clusters.[98,99] The SMSI was initially thought to be an exclusive feature of group VIII metals, characterized by high work function (ϕ) and surface energy. However, it has been recently shown not only that SMSI is also possible for metals with a lower work function or surface energy (γ) such as gold, but in addition, that for the Au/TiO_2 system the SMSI is more likely to occur on large NPs (≈9 and 13 nm) than on small ones (≈3 and 7 nm).[100]

It must be noted that all the above-mentioned examples of catalyst preparation via defect mediated reduction of metal precursors involve noble metals. This is likely due to two main characteristics of noble metals: i) their high reducibility; and ii) the low metal loading that is usually employed for the preparation of such catalysts. Conversely, for a non-noble metal such as Co, which has a negative reduction potential ($Co^{2+} + e^- \rightarrow Co(s)$ ($E° = -0.282$ V)) and is usually employed at high loading (>10 wt%), the role of the defect mediated reduction of ionic precursors during catalyst preparation has not been clarified yet. However, Qiu et al.[101] have recently shown that O_{vac} on TiO_2 can readily reduce pre-synthesized individual Co_3O_4 NPs directly into CoO/Co^0. It is possible to rationalize the impact

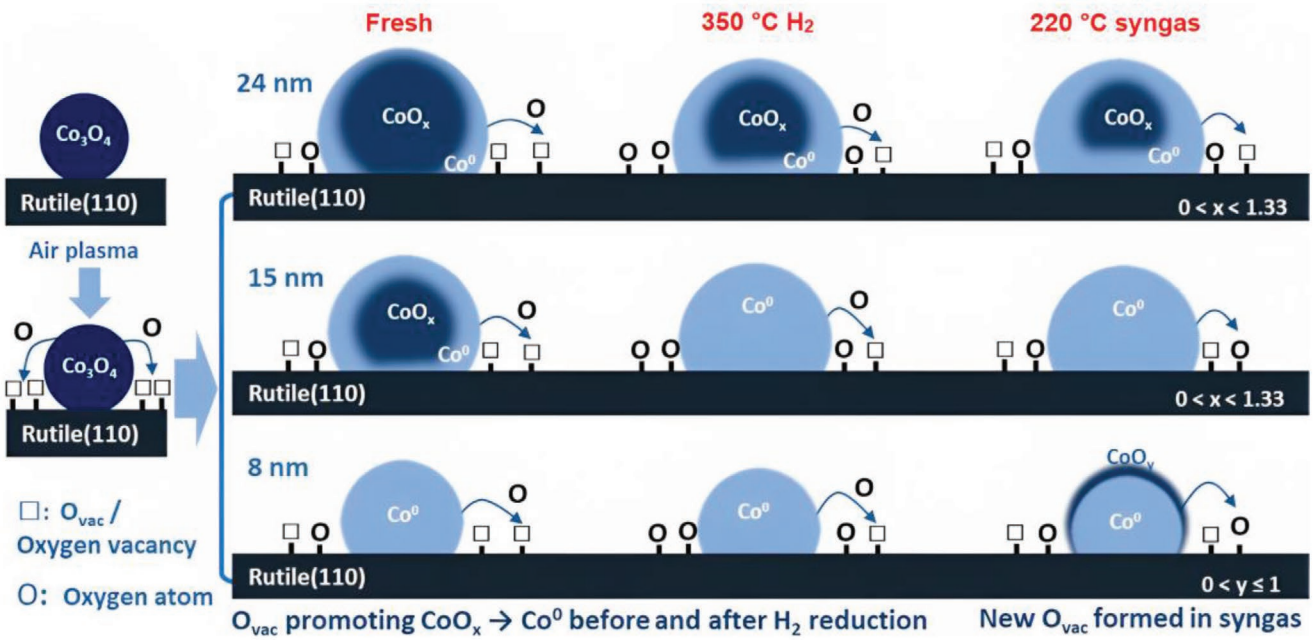

Figure 8. Co_3O_4 NPs reduction into CoO/Co^0 by O_{vac} on rutile substrate and subsequent reductions by H_2 reduction (350 °C) and syngas adsorption (220 °C). Adapted under terms of the CC-BY license.[101] Copyright 2022, The Authors. Published by American Chemical Society.

of O_{vac} on the Co NPs on the base of the standard potentials: $Ti^{4+} + e^- \rightarrow Ti^{3+}$ (–0.56 V); $Co^{2+} + 2e^- \rightarrow Co$ (–0.28 V); and $Co^{3+} + e^- \rightarrow Co^{2+}$ (1.82 V). The potential for the reduction/oxidation of Co/Ti is positive: $Co^{3+} + Ti^{3+} \rightarrow Co^{2+} + Ti^{4+}$ (2.38 V), and $Co^{2+} + 2Ti^{3+} \rightarrow Co + 2Ti^{4+}$ (0.84 V). Thus, the reduction of Co^{3+} to Co^{2+} and Co^{2+} to Co^0 by surface O_{vac}/Ti^{3+} is spontaneous if these species are present in sufficient quantities, and does not need any additional reducing agent.[101] Notably, the extent of the reduction is dependent on the NP size, with smaller particles (<8 nm) being more reduced than the larger ones. Indeed, O_{vac} are particularly good at reducing the edges of larger particles, while the core remains partially oxidized (**Figure 8**).

The latter can be further reduced after H_2 and syngas treatments, accompanied by the consumption of O_{vac} after H_2 exposure. Conversely, an increase in the amount of O_{vac} is observed after the treatment in syngas. Finally, O_{vac} prevents the complete reoxidation of small Co NPs (>8 nm) during syngas exposure.[101]

Therefore, introduction of O_{vac} on reducible supports is a promising and straightforward method to develop new catalytic materials with higher reducibility and stability. Moreover, the combination of such synthetic strategy with careful post-synthesis treatments may promote the formation of specific metal-support interfaces with superior performance for CO_2 hydrogenation.

4.3. SMSI Evolution for Co/TiO_2 Catalysts

Since the first report of SMSI in 1978 by Tauster et al.,[102] great interest toward this effect arose in the catalysis community. In the earlier studies, SMSI was characterized by the inhibition of CO and H_2 chemisorption on group VIII metals supported on TiO_2 after a high temperature reduction.[98] The SMSI effect was explained as an electron transfer between the support and the metal. Nowadays, it is clear that SMSI can promote three different effects: i) electronic; ii) geometric; and iii) bifunctional.[98] The electronic effect consists in the charge redistribution that can occur at the interface between the metal and the support. The degree of electron transfer depends on different factors, spanning from the surface defects on the oxide to the size of the metal clusters.[98] The geometric effect involves a partial (decoration) or total (encapsulation) covering of the metal clusters surface by a TiO_x layer, usually after high temperature reduction (450–500 °C).[98] The commonly accepted two-step encapsulation mechanism involves first the mass transport of interstitial Ti cations (Ti^{n+}, $n = 3,4$) near the surface region, promoted by the high diffusivity of Ti in TiO_2 at high temperatures. To fulfill such step, the work function of the metal must be higher than that of TiO_2 ($\phi_{TiO2(110)} \approx 5.2$ eV).[99] The second step involves the mass transport of TiO_x ($x < 2$) onto the surface of the metallic cluster. Metals with higher surface energy (γ_M) than the one of the oxides are required ($\gamma_M > \gamma_{TiOx}$).[98,99] Therefore, reduced or n-type doped oxides with small surface energies favor encapsulation.[99] The geometric effect can also induce morphological changes in the metals. Indeed, metal particles can be flattened and stabilized on the partially reduced surface of the oxide support.[98,103] The bifunctional effect involves the creation of new reaction sites at the boundary between the metal and the support. These new sites show completely different properties in terms of lattice constant, electron density and composition, which can significantly modify the catalytic activity and the selectivity. The bifunctional effect includes the possibility for the reactive species to migrate or spillover either from the metal or the support to the boundary or edge where the chemical reactions takes place.[98]

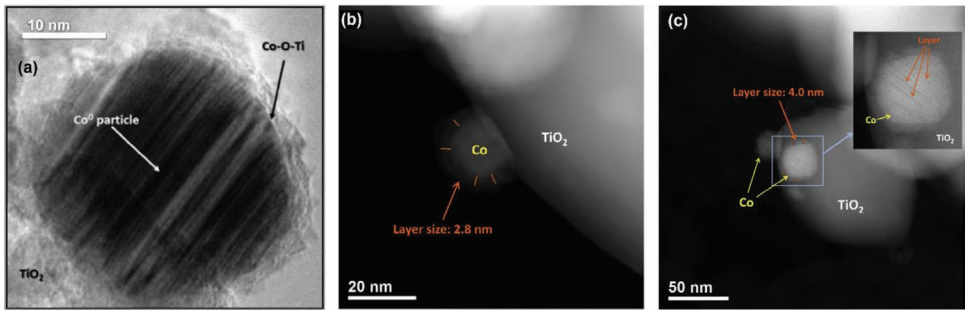

Figure 9. a) HRTEM images of a Co/TiO_2 catalyst depicting the decoration of Co metal NPs by an amorphous TiO_2 layer. Adapted with permission.[104] Copyright 2011, Royal Society of Chemistry. STEM images of b) Co/TiO_2 reduced at 600 °C (layer size: 2.8 nm) c) Co/TiO_2 calcined and reduced at 600 °C (layer size: 4.0 nm). Adapted with permission.[105] Copyright 2015, Elsevier.

However, our comprehension of the SMSI is continuously evolving over the years. For instance, transition metals with small work function or low surface energies such as Cu, Ag, Au, and Co were initially thought to withstand encapsulation,[99] while recent studies have shown that decoration and encapsulation are possible also for these and other metals. Direct evidence of the SMSI encapsulation effect in a 10 wt% Co/TiO_2 (pure anatase) catalyst was highlighted by TEM imaging by De la Peña et al.[104] After high temperature reduction (500 °C, 2 h), two types of cobalt NPs were identified on this sample: i) partially encapsulated Co^0 NPs; and ii) Co^0 NPs covered by a TiO_x amorphous overlayer with a thickness of a few angstroms. Some of these encapsulated Co NPs show some fringes due to the non-epitaxial growth between the metal and the support (**Figure 9**a). Moreover, the formation of Co—O—Ti bonds and the suppression of CO hydrogenation activity during FTS catalytic tests confirm the presence of SMSI. Similar results were obtained also by Lee et al.[105] on a catalyst containing ≈5 wt% of Co supported on commercial TiO_2-P25. A TiO_x layer showing striations and a thickness between 2.8 and 4.0 nm is formed after high temperature calcination and reduction (Figure 9b,c). Characterizations unveiled that the formation of the TiO_x layer occurs already on the Co_3O_4 particles during the calcination step (300–400 °C). The reduction to metallic Co can be complete or only superficial, depending on the reduction temperature, and the final thickness of the TiO_x layer is largely influenced by the treatment conditions.

To study the influence of different support phases on the extension of SMSI, Bertella et al. prepared Ru-promoted Co catalysts (0.5 wt% Ru, 10 wt% Co) on both anatase and rutile TiO_2 for CO-FTS.[106] According to this study, the extent of SMSI decoration is more significant for Co supported on anatase. Moreover, on the anatase based catalyst, the SMSI is partially reversible during the FTS reaction (220 °C, 20 bar, $H_2/CO = 2$). Most of the previously mentioned studies are performed on traditional Co/TiO_2 catalysts, in form of powder or pellets, with particles in close proximity resulting from the high metal loading (up to 20 wt%). Consequently, the characterization of the SMSI and its evolution during the different synthesis steps and post-synthesis treatments is extremely difficult. To have a better understanding of the SMSI evolution in cobalt-based catalysts, Qiu et al. prepared two well-defined model cobalt samples using flat single crystal SiO_xSi (110) and rutile-TiO_2 (110) supports, covered by a monolayer of highly monodispersed Co NPs with a large inter-particle distance (>100 nm).[107] A combination of surface sensitive spectroscopic and microscopic methods was employed to characterize the evolution of MSI during reduction-oxidation-reduction (ROR) treatments. Such treatments are commonly used industrially to regenerate or enhance the catalytic activity by improving metal dispersion, reducibility and MSI.[62,107–110] Weak interactions on SiO_xSi allow the complete reduction of Co NPs, although they migrate and agglomerate during ROR (reduction at 350 or 500 °C, oxidation at 300 °C). In contrast, stronger MSI on TiO_2 leads to only partial reduction of surface exposed cobalt. Moreover, SMSI over TiO_2 avoids the agglomeration of Co NPs, which can however spread on the support and eventually assume a fried-egg-like shape (**Figure 10**).[107]

Such a spreading increases the exposed surface area of Co NPs and their overall electronic state, both of which may affect catalytic activity and selectivity. Nonetheless, if the spreading becomes extensive, this can lead to non-reducible $CoTiO_3$ species, which may be detrimental to reactions involving metallic cobalt as an active phase.[107]

5. Effect of Promoters

Promoters are crucial for FTS catalysts, as they can enhance activity, stability and selectivity.[5] Co-based FTS catalysts usually contain noble metal promoters,[5,111] which can promote the reduction of metal oxides into active metal particles, thus lowering the temperature during the activation and regeneration procedures, and limiting oxidation during the FTS.[111] Moreover, noble metal promotion can also affect the catalytic properties under relevant FTS conditions. The activity usually benefits from noble metal addition, while the effects on C_{5+} selectivity can be highly dependent on the promoter used.[112] Alkaline promoters can decrease the selectivity to methane, by favoring the formation of higher hydrocarbons, along with an increase of olefin concentration in the gasoline product fraction.[113] The addition of alkaline promoters is even more important during CO_2-FTS. Indeed, such promoters, having high basicity, can enhance CO_2 adsorption, thus limiting the formation of CH_4 and increasing C_{5+} selectivity.[114,115] According to Li et al.,[30] the addition of K decreases the difference in catalytic performances between unsupported hcp- and fcc-Co phases. CO_2 conversion increases over both K-hcp-Co and K-fcc-Co, reaching similar

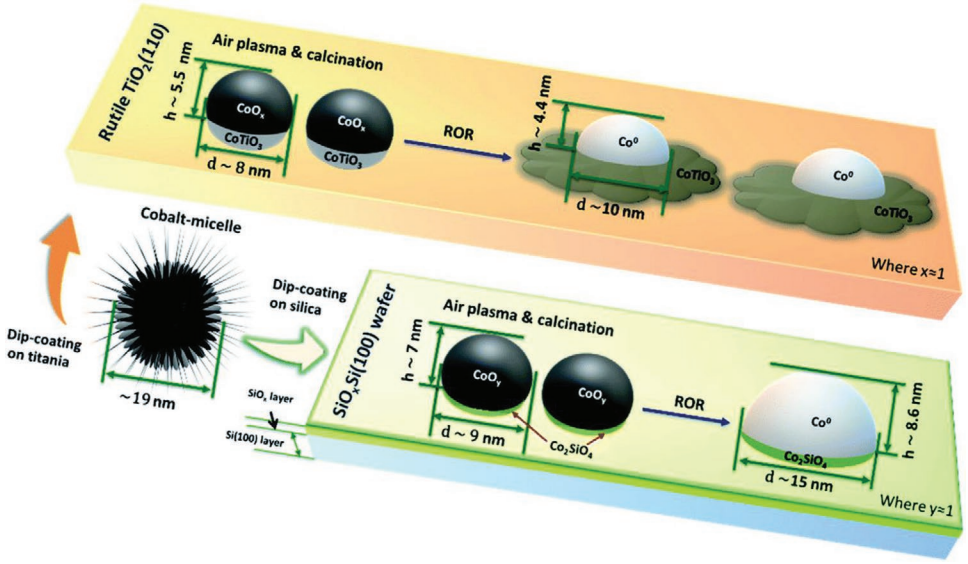

Figure 10. Outline of the Co NP evolution on TiO_2(110) and SiO_xSi(100) supports after ROR. The spreading of Co NPs onto the surface of TiO_2 forms a fried-egg shape resulting in strong interaction with the support to produce $CoTiO_3$, while Co NPs on SiO_xSi tend to move and agglomerate into bigger particles. Reproduced under terms of CC-BY license.[107] Copyright 2020, The Authors. Published by Royal Society of Chemistry.

values, CO becomes the dominant product and C_{2+} start to be formed, with a selectivity that increases to ≈25% at 400 °C. Potassium addition increases the electron density around Co NPs, strengthening CO_2 adsorption and leading to a different reaction pathway.[30] Similarly, the addition of K to a 15 wt% Co/Al_2O_3 catalyst decreases CH_4 selectivity and increases C_{2+} production, with an optimum K loading of 6 wt%.[116] Promotion by Zr, K, and Cs improves CO_2, CO and H_2 adsorption over anatase- and rutile-TiO_2 supported cobalt catalysts.[20] Zr addition modifies the reaction pathway over anatase-supported catalysts toward formate intermediate species, enabling the subsequent hydrogenation of CO to CH_4 and C_{2+} species. The surface C/H ratio benefits from promoter addition (unpromoted < Zr-promoted < K-Zr-promoted ≈Cs-Zr-promoted) resulting in a higher C_{2+} selectivity (Figure 3).[20]

Alkaline promoters play a pivotal role also for cobalt-based bimetallic catalysts. Indeed, the introduction of metals that are more active for RWGS reaction (e.g., Fe, Cu) can slightly improve the selectivity toward C_{2+} products. Such improvement becomes noticeable when alkaline promoters are combined to the bimetallic catalysts. Shi et al.[114] investigated the CO_2 hydrogenation to long-chain hydrocarbons over a series of K-promoted (0–3.5 wt%) Co-Cu/TiO_2 catalysts. The addition of suitable amounts of K (2.5 wt%) suppresses the CH_4 formation and increases the C_{5+} selectivity. This trend is related to the enhanced CO_2 chemisorption and the reduced H_2 adsorption detected upon K promotion.[114] Similar results were obtained in a follow-up study,[115] where the authors examined the promotion by various alkali metals (Li, Na, K, Rb, and Cs). Among the different catalysts, the Na-promoted Co-Cu/TiO_2, because of its stronger basicity, shows the highest C_{5+} selectivity.[115] Likewise, alkali-promoted Fe-Co catalysts show superior selectivity toward C_{2+} products and negligible CH_4 production.[9,77,117,118] However, such catalysts usually produce more light olefins and present lower overall activity than monometallic Co-based catalysts.[9,10] The improved selectivity originates from the ability of alkali-promoted Fe oxides and carbides to enhance RWGS and CO hydrogenation to C_{2+}, with similar behavior and product distribution than traditional FTS Fe-based catalysts.[9,77,117,118] Indeed, on Fe-based catalysts, Fe_3O_4 is normally responsible for the RWGS reaction, while iron carbides account for C—C coupling via traditional FTS.[8,119] However, during CO_2-FTS, high CH_4 selectivity is obtained for almost all unpromoted iron-based catalysts.[8] Alkali promoters can significantly enhance the formation of longer chain hydrocarbons and olefins in several ways. They can i) promote the carburization of iron species; ii) enhance CO_2 and CO adsorption; iii) suppress H_2 adsorption on the catalyst surface; and/or iv) suppress re-adsorption and re-hydrogenation of olefins.[8,120–124] Therefore, the higher CO/H_2 and CO_2/H_2 ratios promote CO_2 conversion and olefin selectivity.[8] According to Jiang et al.[125] the addition of a small amount of Co to a K-promoted iron-based catalysts can increase both CO_2 conversion and selectivity toward C_{2+} hydrocarbons. Indeed, in such bimetallic Fe-Co catalysts, cobalt can contribute to the increase of the CO conversion via traditional FTS.[125] The intimate contact between the two metals facilitates the spillover of the CO intermediate from the Fe_3O_4 where it is produced via RWGS, to the cobalt sites. Therefore, CO conversion can proceed on both Co and Fe_5C_2 sites.[8,125] However, bimetallic Fe-Co catalysts usually contain larger amount of Fe compared to the one of Co, which acts as a promoter.[117,126] Therefore, a detailed description of such bimetallic catalysts is beyond the scope of this review. The reader can find several detailed reviews concerning CO_2 hydrogenation on Fe-based, as well as comparisons between Co and Fe-based catalysts in the literature.[4,8,127,128]

Besides the increased CO_2 adsorption stemming from the enhanced basicity of the promoted catalytic surface, alkali and alkaline earth promotion can also favor the generation of oxygen vacancies on reducible supports, and improve the final metal dispersion.[129,130] According to Liu et al.,[129] the modification of

a CeO_2 support by the addition of different alkaline earth metal oxides with a M/Ce (M = Mg, Ca, Sr, Ba) molar ration of 1/9 via sol-gel method leads to the formation of more O_{vac} on the final $Ni/M_{0.1}CeO_x$ catalyst. Moreover, such modification increases both strength and number of the moderate alkaline sites and the Ni dispersion.[129]

Finally, noble metal promotion does not improve the selectivity for higher hydrocarbons.[131] The higher surface hydrogenation achievable by the addition of different noble metals can benefit the overall activity and suppress olefin production, however increasing CH_4 selectivity.[131] The dual promotion with transition and alkali metals was proved to be more successful than noble-alkali metal combination: Co-Na-Mo/SiO_2 has similar C_{5+} selectivity to the one of Co-K-Pt/SiO_2 catalysts, albeit with higher conversion.[131]

Hence, the addition of alkali promoters can increase CO_2 adsorption and the intrinsically marginal activity of Co-based catalysts for RWGS, helping to mitigate excess methanation and increase overall C_{2+} selectivity. However, chain-growth probability remains modest even in presence of alkaline promoters, varying from 0.55 to 0.65 in all cases.[2,32]

6. Conclusions

CO_2-FTS-based hydrocarbons could allow the creation of a circular carbon economy with a significant impact on anthropogenic emissions into the atmosphere. Due to their high C—C coupling activity in the conventional FTS process, cobalt-based catalysts are good candidates for direct CO_2 hydrogenation to C_{2+} hydrocarbons. Unfortunately, Co-based catalysts act differently when CO_2 substitutes CO in the feed, producing mainly methane.

This review summarizes the progress achieved toward the single-step hydrogenation of CO_2 to long-chain hydrocarbons over oxide-supported Co-based catalysts under traditional FTS conditions. The main conclusions and perspectives are listed below:

i. Due to weak CO_2 adsorption and RWGS thermodynamic constraints, C/H surface ratio and CO coverage are generally low over Co-based catalysts, leading to the preferential production of CH_4 and short-chain hydrocarbons. Methane formation can be decreased and C_{2+} selectivity can be increased by the careful choice of cobalt active phase, metal oxide support, regulation of the metal-support interfaces and addition of alkaline metal promoters.
ii. Both metallic cobalt and cobalt oxide (CoO) can be the active phase during CO_2-FTS reaction, depending on the support used. Metallic cobalt is more active on most supports, while CoO appears to be a better choice for TiO_2 supports. Such a behavior stems from the formation of a unique interface between the cobalt active phase and the TiO_2 support. Due to its lower hydrogenation ability, CoO/TiO_2 produces less CH_4 and more C_{2+} products compared to its metallic counterpart, with a higher content of olefins. Moreover, CoO shows interesting activity toward the RWGS reaction. Nonetheless, further investigations are needed to clarify the role of CoO and Co^0-CoO interfaces during CO_2-FTS, as well as the possible formation of cobalt carbide and its consequences on CO_2 hydrogenation.
iii. Independently from the cobalt active phase, reducible oxides and especially TiO_2 are better adapted for this reaction than irreducible oxides. The higher activity obtained on TiO_2-based catalysts stems from the ability of reducible oxides to create specific metal-support interfaces, originating from SMSI, which can strongly benefit the CO_2 activation to different products, from C_{2+} to CH_4 and CO. Moreover, reducible oxides and metal-oxide interfaces are rich in surface defects (O_{vac}, Ti^{3+}) that can be exploited for direct activation of CO_2. Providing Co-based catalysts supported on reducible oxides with large number of O_{vac} can be an efficient strategy to increase the activity during CO_2 hydrogenation and tune the selectivity toward the desired products.
iv. The oxygen vacancies can directly interact with metal precursors and affect the evolution of SMSI. The introduction of O_{vac} on reducible supports is a promising and straightforward method to develop new catalytic materials with higher reducibility and stability. Moreover, the combination of such synthetic strategies with careful post-synthesis treatments might promote the formation of specific metal-support interfaces with superior performance for CO_2 hydrogenation.
v. The addition of alkali promoters can increase CO_2 adsorption, C/H surface ratio and the intrinsically marginal activity of Co-based catalysts for RWGS, helping to mitigate excess methanation and to increase overall C_{2+} selectivity. The addition of other transition metals, which favor RWGS (e.g., Cu and Fe) in combination with alkaline promoters can as well improve the overall activity and selectivity. Finally, the modification of reducible supports by alkaline earth metals can promote the formation of O_{vac}.
vi. Despite the application of the above-mentioned strategies, chain growth probability (α) remains limited by the low CO fugacity and consequent surface coverage (θ_{CO}). Therefore, Co-based catalysts might be used, under pure CO_2/H_2 feeds, for the direct production of synthetic natural gas mixture rich in light C_2-C_4 hydrocarbons and CO_2-based middle distillate mix (i.e., gasoline, jet fuel, diesel), without the necessity of a downstream hydrocracking refining treatment. Further improvements of the product distribution (higher α) can be obtained via utilization of mixed $CO/CO_2/H_2$ feeds (e.g., the ones resulting from biomass gasification), which can ensure higher θ_{CO}.
vii. Further implementation of Co-based catalysts for CO_2 hydrogenation should be focused, first of all, on the clarification of cobalt particle size effect. Then, the activity of hcp-Co supported on reducible TiO_2 should be investigated. Finally, due to the pivotal role played by the support on the activation of CO_2, large efforts should be devoted to the development of an extremely active TiO_2 support, rich in O_{vac} and alkaline promoters, to ensure proper CO_2 activation and metal-interface formation.

Acknowledgements

This work was supported by the Agence Nationale de la Recherche (project ANR-19-CE07-0030), which is gratefully acknowledged.

Conflict of Interest

The authors declare no conflict of interest.

Keywords

CO_2 hydrogenation, cobalt catalysts, liquid fuels, metal oxides, metal-support interaction, oxygen vacancy, promoters

Received: January 3, 2023
Revised: March 7, 2023
Published online:

[1] I. Hussain, G. Tanimu, S. Ahmed, C. U. Aniz, H. Alasiri, K. Alhooshani, *Int. J. Hydrogen Energy* **2022**, https://doi.org/10.1016/j.ijhydene.2022.08.086.
[2] G. Prieto, *ChemSusChem* **2017**, *10*, 1056.
[3] I. C. T. Have, J. J. G. Kromwijk, M. Monai, D. Ferri, E. B. Sterk, F. Meirer, B. M. Weckhuysen, *Nat. Commun.* **2022**, *13*, 324.
[4] R.-P. Ye, J. Ding, W. Gong, M. D. Argyle, Q. Zhong, Y. Wang, C. K. Russell, Z. Xu, A. G. Russell, Q. Li, M. Fan, Y.-G. Yao, *Nat. Commun.* **2019**, *10*, 5698.
[5] T. Lin, Y. An, F. Yu, K. Gong, H. Yu, C. Wang, Y. Sun, L. Zhong, *ACS Catal.* **2022**, *12*, 12092.
[6] W. W. Russell, G. H. Miller, *J. Am. Chem. Soc.* **1950**, *72*, 2446.
[7] W. Liu, S. Cheng, H. S. Malhi, X. Gao, Z. Zhang, W. Tu, *Catalysts* *12*, 1432.
[8] J. Liu, Y. Song, X. Guo, C. Song, X. Guo, *Chin. J. Catal.* **2022**, *43*, 731.
[9] L. Zhang, Y. Dang, X. Zhou, P. Gao, A. Petrus van Bavel, H. Wang, S. Li, L. Shi, Y. Yang, E. I. Vovk, Y. Gao, Y. Sun, *The Innovation* **2021**, *2*, 100170.
[10] F. Yuan, G. Zhang, J. Zhu, F. Ding, A. Zhang, C. Song, X. Guo, *Catal. Today* **2021**, *371*, 142.
[11] T. Riedel, M. Claeys, H. Schulz, G. Schaub, S.-S. Nam, K.-W. Jun, M.-J. Choi, G. Kishan, K.-W. Lee, *Appl. Catal., A* **1999**, *186*, 201.
[12] R. W. Dorner, D. R. Hardy, F. W. Williams, B. H. Davis, H. D. Willauer, *Energy Fuels* **2009**, *23*, 4190.
[13] C. G. Visconti, M. Martinelli, L. Falbo, L. Fratalocchi, L. Lietti, *Catal. Today* **2016**, *277*, 161.
[14] U. Rodemerck, M. Holeňa, E. Wagner, Q. Smejkal, A. Barkschat, M. Baerns, *ChemCatChem* **2013**, *5*, 1948.
[15] J. P. den Breejen, P. B. Radstake, G. L. Bezemer, J. H. Bitter, V. Frøseth, A. Holmen, K. P. de Jong, *J. Am. Chem. Soc.* **2009**, *131*, 7197.
[16] C. J. Weststrate, J. van de Loosdrecht, J. W. Niemantsverdriet, *J. Catal.* **2016**, *342*, 1.
[17] M. Zhuo, A. Borgna, M. Saeys, *J. Catal.* **2013**, *297*, 217.
[18] D. Hibbitts, E. Dybeck, T. Lawlor, M. Neurock, E. Iglesia, *J. Catal.* **2016**, *337*, 91.
[19] P. Bredy, D. Farrusseng, Y. Schuurman, F. C. Meunier, *J. Catal.* **2022**, *411*, 93.
[20] W. Li, G. Zhang, X. Jiang, Y. Liu, J. Zhu, F. Ding, Z. Liu, X. Guo, C. Song, *ACS Catal.* **2019**, *9*, 2739.
[21] I. C. ten Have, B. M. Weckhuysen, *Chem Catalysis* **2021**, *1*, 339.
[22] Z. Qi, L. Chen, S. Zhang, J. Su, G. A. Somorjai, *Appl. Catal., A* **2020**, *602*, 117701.
[23] V. A. de la Peña O'Shea, I. D. P. R. Moreira, A. Roldán, F. Illas, *J. Chem. Phys.* **2010**, *133*, 024701.
[24] D. P. Dinega, M. G. Bawendi, *Angew. Chem., Int. Ed.* **1999**, *38*, 1788.
[25] V. F. Puntes, K. M. Krishnan, A. P. Alivisatos, *Science* **2001**, *291*, 2115.
[26] T. W. van Deelen, H. Su, N. A. J. M. Sommerdijk, K. P. de Jong, *Chem. Commun.* **2018**, *54*, 2530.
[27] R. Lizárraga, F. Pan, L. Bergqvist, E. Holmström, Z. Gercsi, L. Vitos, *Sci. Rep.* **2017**, *7*, 3778.
[28] O. Kitakami, H. Sato, Y. Shimada, F. Sato, M. Tanaka, *Phys. Rev. B* **1997**, *56*, 13849.
[29] Z. Gholami, Z. Tišler, V. Rubáš, *Catal. Rev.* **2021**, *63*, 512.
[30] W. Li, X. Nie, H. Yang, X. Wang, F. Polo-Garzon, Z. Wu, J. Zhu, J. Wang, Y. Liu, C. Shi, C. Song, X. Guo, *Appl. Catal., B* **2022**, *315*, 121529.
[31] V. Iablokov, S. K. Beaumont, S. Alayoglu, V. V. Pushkarev, C. Specht, J. Gao, A. P. Alivisatos, N. Kruse, G. A. Somorjai, *Nano Lett.* **2012**, *12*, 3091.
[32] R. E. Owen, P. Plucinski, D. Mattia, L. Torrente-Murciano, V. P. Ting, M. D. Jones, *J. CO2 Util.* **2016**, *16*, 97.
[33] G. Melaet, W. T. Ralston, C.-S. Li, S. Alayoglu, K. An, N. Musselwhite, B. Kalkan, G. A. Somorjai, *J. Am. Chem. Soc.* **2014**, *136*, 2260.
[34] M.-R. Li, G.-C. Wang, *J. Catal.* **2018**, *365*, 391.
[35] M. Wang, G. Zhang, J. Zhu, W. Li, J. Wang, K. Bian, Y. Liu, F. Ding, C. Song, X. Guo, *Chem. Eng. J.* **2022**, *446*, 137217.
[36] S. Liu, Y. He, W. Fu, J. Chen, J. Ren, L. Liao, R. Sun, Z. Tang, C. Mebrahtu, F. Zeng, *J. CO2 Util.* **2023**, *67*, 102322.
[37] A. Efremova, T. Rajkumar, Á. Szamosvölgyi, A. Sápi, K. Baán, I. Szenti, J. Gómez-Pérez, G. Varga, J. Kiss, G. Halasi, Á. Kukovecz, Z. Kónya, *J. Phys. Chem. C* **2021**, *125*, 7130.
[38] Y. Lian, T. Fang, Y. Zhang, B. Liu, j. Li, *J. Catal.* **2019**, *379*, 46.
[39] K. Zhao, M. Calizzi, E. Moioli, M. Li, A. Borsay, L. Lombardo, R. Mutschler, W. Luo, A. Züttel, *J Energy Chem* **2021**, *53*, 241.
[40] K. Deng, L. Lin, N. Rui, D. Vovchok, F. Zhang, S. Zhang, S. D. Senanayake, T. Kim, J. A. Rodriguez, *Catal. Sci. Technol.* **2020**, *10*, 6468.
[41] N. H. M. D. Dostagir, R. Rattanawan, M. Gao, J. Ota, J.-Y. Hasegawa, K. Asakura, A. Fukouka, A. Shrotri, *ACS Catal.* **2021**, *11*, 9450.
[42] T. Lin, F. Yu, Y. An, T. Qin, L. Li, K. Gong, L. Zhong, Y. Sun, *Acc. Chem. Res.* **2021**, *54*, 1961.
[43] Y.-P. Pei, J.-X. Liu, Y.-H. Zhao, Y.-J. Ding, T. Liu, W.-D. Dong, H.-J. Zhu, H.-Y. Su, L. Yan, J.-L. Li, W.-X. Li, *ACS Catal.* **2015**, *5*, 3620.
[44] Z. Zhao, W. Lu, R. Yang, H. Zhu, W. Dong, F. Sun, Z. Jiang, Y. Lyu, T. Liu, H. Du, Y. Ding, *ACS Catal.* **2018**, *8*, 228.
[45] P. Wang, S. Wei, K. Sun, J. Li, C. He, Y. Xu, X. Du, Y. Tan, Y. Wu, X. Gao, *Ind. Eng. Chem. Res.* **2022**, *61*, 3900.
[46] T.-y. Chen, J. Su, Z. Zhang, C. Cao, X. Wang, R. Si, X. Liu, B. Shi, J. Xu, Y.-F. Han, *ACS Catal.* **2018**, *8*, 8606.
[47] W.-G. Cui, Y.-T. Li, H. Zhang, Z.-C. Wei, B.-H. Gao, J.-J. Dai, T.-L. Hu, *Appl. Catal., B* **2020**, *278*, 119262.
[48] S. Zhang, X. Liu, Z. Shao, H. Wang, Y. Sun, *J. Catal.* **2020**, *382*, 86.
[49] L. Zhong, F. Yu, Y. An, Y. Zhao, Y. Sun, Z. Li, T. Lin, Y. Lin, X. Qi, Y. Dai, L. Gu, J. Hu, S. Jin, Q. Shen, H. Wang, *Nature* **2016**, *538*, 84.
[50] R. Yang, Z. Xia, Z. Zhao, F. Sun, X. Du, H. Yu, S. Gu, L. Zhong, J. Zhao, Y. Ding, Z. Jiang, *J. Energy Chem.* **2019**, *32*, 118.
[51] J. G. Moya-Cancino, A.-P. Honkanen, A. M. J. van der Eerden, R. Oord, M. Monai, I. ten Have, C. J. Sahle, F. Meirer, B. M. Weckhuysen, F. M. F. de Groot, S. Huotari, *ACS Catal.* **2021**, *11*, 809.
[52] Y.-H. Zhao, H.-Y. Su, K. Sun, J. Liu, W.-X. Li, *Surf. Sci.* **2012**, *606*, 598.
[53] N. E. Tsakoumis, M. Rønning, Ø. Borg, E. Rytter, A. Holmen, *Catal. Today* **2010**, *154*, 162.
[54] Y. Yu, S. Mottaghi-Tabar, M. W. Iqbal, A. Yu, D. S. A. Simakov, *Catal. Today* **2021**, *379*, 250.
[55] P. R. Khangale, R. Meijboom, K. Jalama, *Catal. Lett.* **2021**, *151*, 3396.
[56] S. Zhang, X. Liu, H. Luo, Z. Wu, B. Wei, Z. Shao, C. Huang, K. Hua, L. Xia, J. Li, L. Liu, W. Ding, H. Wang, Y. Sun, *ACS Catal.* **2022**, *12*, 8544.
[57] S. Zhang, C. Huang, Z. Shao, H. Zhou, J. Chen, L. Li, J. Lu, X. Liu, H. Luo, L. Xia, H. Wang, Y. Sun, *ACS Catal.* **2023**, *13*, 3055.

[58] R. Munirathinam, D. P. Minh, A. Nzihou, *Ind. Eng. Chem. Res.* **2018**, *57*, 16137.
[59] Y. Zhang, X. Yang, X. Yang, H. Duan, H. Qi, Y. Su, B. Liang, H. Tao, B. Liu, D. Chen, X. Su, Y. Huang, T. Zhang, *Nat. Commun.* **2020**, *11*, 3185.
[60] Y. Zhang, X. Su, L. Li, H. Qi, C. Yang, W. Liu, X. Pan, X. Liu, X. Yang, Y. Huang, T. Zhang, *ACS Catal.* **2020**, *10*, 12967.
[61] P. M. Maitlis, V. Zanotti, *Chem. Commun.* **2009**, 1619.
[62] C. Hernández Mejía, T. W. van Deelen, K. P. de Jong, *Nat. Commun.* **2018**, *9*, 4459.
[63] S. Huygh, A. Bogaerts, E. C. Neyts, *J. Phys. Chem. C* **2016**, *120*, 21659.
[64] J. Szanyi, J. H. Kwak, *Phys. Chem. Chem. Phys.* **2014**, *16*, 15117.
[65] J. C. Lavalley, *Catal. Today* **1996**, *27*, 377.
[66] W. Karim, C. Spreafico, A. Kleibert, J. Gobrecht, J. VandeVondele, Y. Ekinci, J. A. van Bokhoven, *Nature* **2017**, *541*, 68.
[67] M. Kantcheva, M. U. Kucukkal, S. Suzer, *J. Catal.* **2000**, *190*, 144.
[68] A. Aguirre, S. E. Collins, *Catal. Today* **2013**, *205*, 34.
[69] W. L. Vrijburg, E. Moioli, W. Chen, M. Zhang, B. J. P. Terlingen, B. Zijlstra, I. A. W. Filot, A. Züttel, E. A. Pidko, E. J. M. Hensen, *ACS Catal.* **2019**, *9*, 7823.
[70] A. Kim, C. Sanchez, G. Patriarche, O. Ersen, S. Moldovan, A. Wisnet, C. Sassoye, D. P. Debecker, *Catal. Sci. Technol.* **2016**, *6*, 8117.
[71] P. R. Khangale, *Catal. Lett.* **2022**, *152*, 2745.
[72] A. Parastaev, V. Muravev, E. Huertas Osta, A. J. F. van Hoof, T. F. Kimpel, N. Kosinov, E. J. M. Hensen, *Nat. Catal.* **2020**, *3*, 526.
[73] J. Díez-Ramírez, P. Sánchez, V. Kyriakou, S. Zafeiratos, G. E. Marnellos, M. Konsolakis, F. Dorado, *J. CO2 Util.* **2017**, *21*, 562.
[74] S. Kattel, P. Liu, J. G. Chen, *J. Am. Chem. Soc.* **2017**, *139*, 9739.
[75] T. Pu, W. Zhang, M. Zhu, *Angew. Chem., Int. Ed.* **2022**, *63*, e202212278.
[76] U. J. Etim, C. Zhang, Z. Zhong, *Nanomaterials* **2021**, *11*, 3265.
[77] T. Fan, H. Liu, S. Shao, Y. Gong, G. Li, Z. Tang, *J. Phys. Chem. Lett.* **2021**, *12*, 10486.
[78] Z. Zhang, X. Zhang, L. Zhang, J. Gao, Y. Shao, D. Dong, S. Zhang, Q. Liu, L. Xu, X. Hu, *J. Energy Inst.* **2020**, *93*, 1581.
[79] P. C. D. Mendes, L. G. Verga, J. L. F. Da Silva, *Phys. Chem. Chem. Phys.* **2021**, *23*, 6029.
[80] H. Yu, D. Cao, A. Fisher, R. L. Johnston, D. Cheng, *Appl. Surf. Sci.* **2017**, *396*, 539.
[81] J. Niu, J. Ran, Z. Ou, X. Du, R. Wang, W. Qi, P. Zhang, *J. CO2 Util.* **2016**, *16*, 431.
[82] J. Jia, C. Qian, Y. Dong, Y. F. Li, H. Wang, M. Ghoussoub, K. T. Butler, A. Walsh, G. A. Ozin, *Chem. Soc. Rev.* **2017**, *46*, 4631.
[83] Z. Cheng, B. J. Sherman, C. S. Lo, *J. Chem. Phys.* **2013**, *138*, 014702.
[84] J. Lee, D. C. Sorescu, X. Deng, *J. Am. Chem. Soc.* **2011**, *133*, 10066.
[85] S. Chen, T. Cao, Y. Gao, D. Li, F. Xiong, W. Huang, *J. Phys. Chem. C* **2016**, *120*, 21472.
[86] S. Kattel, B. Yan, J. G. Chen, P. Liu, *J. Catal.* **2016**, *343*, 115.
[87] L. F. Bobadilla, J. L. Santos, S. Ivanova, J. A. Odriozola, A. Urakawa, *ACS Catal.* **2018**, *8*, 7455.
[88] A. R. Puigdollers, P. Schlexer, S. Tosoni, G. Pacchioni, *ACS Catal.* **2017**, *7*, 6493.
[89] Z.-Y. Pu, X.-S. Liu, A.-P. Jia, Y.-L. Xie, J.-Q. Lu, M.-F. Luo, *J. Phys. Chem. C* **2008**, *112*, 15045.
[90] A. Sarkar, G. G. Khan, *Nanoscale* **2019**, *11*, 3414.
[91] M. Xing, W. Fang, M. Nasir, Y. Ma, J. Zhang, M. Anpo, *J. Catal.* **2013**, *297*, 236.
[92] W. Fang, M. Xing, J. Zhang, *Appl. Catal., B* **2014**, *160–161*, 240.
[93] X. Pan, M.-Q. Yang, X. Fu, N. Zhang, Y.-J. Xu, *Nanoscale* **2013**, *5*, 3601.
[94] G. Xi, J. Ye, Q. Ma, N. Su, H. Bai, C. Wang, *J. Am. Chem. Soc.* **2012**, *134*, 6508.
[95] X. Pan, Y.-J. Xu, *Appl. Catal., A* **2013**, *459*, 34.
[96] X. Pan, Y.-J. Xu, *J. Phys. Chem. C* **2013**, *117*, 17996.
[97] F. Cao, Z. Song, Z. Zhang, Y.-S. Xiao, M. Zhang, X. Hu, Z.-W. Liu, Y. Qu, *ACS Appl. Mater. Interfaces* **2021**, *13*, 24957.
[98] C.-J. Pan, M.-C. Tsai, W.-N. Su, J. Rick, N. G. Akalework, A. K. Agegnehu, S.-Y. Cheng, B.-J. Hwang, *J. Taiwan Inst. Chem. Eng.* **2017**, *74*, 154.
[99] Q. Fu, T. Wagner, S. Olliges, H.-D. Carstanjen, *J. Phys. Chem. B* **2005**, *109*, 944.
[100] X. Du, Y. Huang, X. Pan, B. Han, Y. Su, Q. Jiang, M. Li, H. Tang, G. Li, B. Qiao, *Nat. Commun.* **2020**, *11*, 5811.
[101] C. Qiu, Y. Odarchenko, Q. Meng, S. Xu, I. Lezcano-Gonzalez, P. Olalde-Velasco, F. Maccherozzi, L. Zanetti-Domingues, M. Martin-Fernandez, A. M. Beale, *ACS Catal.* **2022**, *12*, 9125.
[102] S. J. Tauster, S. C. Fung, R. L. Garten, *J. Am. Chem. Soc.* **1978**, *100*, 170.
[103] V. M. Gonzalez-DelaCruz, J. P. Holgado, R. Pereñíguez, A. Caballero, *J. Catal.* **2008**, *257*, 307.
[104] V. A. de la Peña O'Shea, M. C. Álvarez Galván, A. E. P. Prats, J. M. Campos-Martin, J. L. G. Fierro, *Chem. Commun.* **2011**, *47*, 7131.
[105] J. Lee, S. P. Burt, C. A. Carrero, A. C. Alba-Rubio, I. Ro, B. J. O'Neill, H. J. Kim, D. H. K. Jackson, T. F. Kuech, I. Hermans, J. A. Dumesic, G. W. Huber, *J. Catal.* **2015**, *330*, 19.
[106] F. Bertella, P. Concepción, A. Martínez, *Catal. Today* **2017**, *289*, 181.
[107] C. Qiu, Y. Odarchenko, Q. Meng, P. Cong, M. A. W. Schoen, A. Kleibert, T. Forrest, A. M. Beale, *Chem. Sci.* **2020**, *11*, 13060.
[108] M. M. Hauman, A. Saib, D. J. Moodley, E. du Plessis, M. Claeys, E. van Steen, *ChemCatChem* **2012**, *4*, 1411.
[109] L. Tang, D. Yamaguchi, B. Leita, V. Sage, N. Burke, K. Chiang, *Catal. Commun.* **2015**, *59*, 166.
[110] J. Cai, F. Jiang, X. Liu, *Appl. Catal., B* **2017**, *210*, 1.
[111] J. Horáček, *Monatsh. Chem.* **2020**, *151*, 649.
[112] T. O. Eschemann, J. Oenema, K. P. de Jong, *Catal. Today* **2016**, *261*, 60.
[113] O. L. Eliseev, M. V. Tsapkina, O. S. Dement'eva, P. E. Davydov, A. V. Kazakov, A. L. Lapidus, *Kinet. Catal.* **2013**, *54*, 207.
[114] Z. Shi, H. Yang, P. Gao, X. Li, L. Zhong, H. Wang, H. Liu, W. Wei, Y. Sun, *Catal. Today* **2018**, *311*, 65.
[115] Z. Shi, H. Yang, P. Gao, X. Chen, H. Liu, L. Zhong, H. Wang, W. Wei, Y. Sun, *Chin. J. Catal.* **2018**, *39*, 1294.
[116] P. R. Khangale, R. Meijboom, K. Jalama, *J. CO2 Util.* **2020**, *41*, 101268.
[117] R. Satthawong, N. Koizumi, C. Song, P. Prasassarakich, *J. CO2 Util.* **2013**, *3–4*, 102.
[118] P. Gao, L. Zhang, S. Li, Z. Zhou, Y. Sun, *ACS Cent. Sci.* **2020**, *6*, 1657.
[119] P. Kangvansura, L. M. Chew, C. Kongmark, P. Santawaja, H. Ruland, W. Xia, H. Schulz, A. Worayingyong, M. Muhler, *Engineering* **2017**, *3*, 385.
[120] Q. Chang, C. Zhang, C. Liu, Y. Wei, A. V. Cheruvathur, A. I. Dugulan, J. W. Niemantsverdriet, X. Liu, Y. He, M. Qing, L. Zheng, Y. Yun, Y. Yang, Y. Li, *ACS Catal.* **2018**, *8*, 3304.
[121] B. Liang, H. Duan, T. Sun, J. Ma, X. Liu, J. Xu, X. Su, Y. Huang, T. Zhang, *ACS Sustainable Chem. Eng.* **2019**, *7*, 925.
[122] J. Wang, Z. You, Q. Zhang, W. Deng, Y. Wang, *Catal. Today* **2013**, *215*, 186.
[123] R. Satthawong, N. Koizumi, C. Song, P. Prasassarakich, *Catal. Today* **2015**, *251*, 34.
[124] T. Numpilai, N. Chanlek, Y. Poo-Arporn, C. K. Cheng, N. Siri-Nguan, T. Sornchamni, M. Chareonpanich, P. Kongkachuichay, N. Yigit, G. Rupprechter, J. Limtrakul, T. Witoon, *ChemCatChem* **2020**, *12*, 3306.
[125] F. Jiang, B. Liu, S. Geng, Y. Xu, X. Liu, *Catal. Sci. Technol.* **2018**, *8*, 4097.

[126] M. Ronda-Lloret, G. Rothenberg, N. R. Shiju, *ChemSusChem* **2019**, *12*, 3896.
[127] D. D. Suppiah, W. M. A. W. Daud, M. R. Johan, *Energy Fuels* **2021**, *35*, 17261.
[128] T. A. Atsbha, T. Yoon, P. Seongho, C.-J. Lee, *J. CO2 Util.* **2021**, *44*, 101413.
[129] K. Liu, X. Xu, J. Xu, X. Fang, L. Liu, X. Wang, *J. CO2 Util.* **2020**, *38*, 113.
[130] A. I. Tsiotsias, N. D. Charisiou, I. V. Yentekakis, M. A. Goula, *Catalysts 10*, 812.
[131] R. E. Owen, J. P. O'Byrne, D. Mattia, P. Plucinski, S. I. Pascu, M. D. Jones, *Chem. Commun.* **2013**, *49*, 11683.

Canio Scarfiello obtained his bachelor's and master's degree in industrial chemistry from the Sapienza University of Rome. He is currently developing his Ph.D. research on carbon dioxide hydrogenation to liquid fuels at the RAPSODEE, LPCNO and LCC laboratories.

Doan Pham Minh received his Ph.D. degree in chemistry at the University Lyon 1, France in 2006. He is currently full professor and deputy director of the RAPSODEE research center, UMR CNRS 5302 at IMT Mines Albi. His research is focused on the design of new performing catalysts for applications in the production of green hydrogen, biomethane, and biofuels, as well as on the development of refractory ceramics and processes for high temperature sensible heat storage.

Katerina Soulantica received her Ph.D. in chemistry from the University of Athens (Greece) in 1995. From 1995 to 1998 she was a post-doctoral fellow in Spain (Prof. P. Espinet, Valladolid). In 1999, she joined the group of Dr. B. Chaudret at the LCC (Toulouse). In 2005, she joined the LPCNO laboratory as a research associate and since 2008 she is a CNRS researcher in the nanostructures and organometallic chemistry (NOC) group of LPCNO. Her research domain is the synthesis of metal nanoparticles and their applications in microelectronics, biodetection, and catalysis.

Philippe Serp is a professor of inorganic chemistry in Toulouse University. He received his Ph.D. degree from Toulouse University in 1994 and engaged in postdoctoral research at the University of Porto and Louvain-la-Neuve from 1995 to 1997. His research interests in the laboratory of coordination chemistry include the preparation of nanostructured catalytic materials, and molecular approaches to understand supported catalysis; fields in which with co-workers he has published over 200 papers among them twenty European and U.S. patents. His research has been recognized by the Catalysis (2004) and Industrial Chemistry (2012) Division Awards of the French Chemical Society.